Coronagraph Design Optimization for Segmented Aperture Telescopes

Jeffrey Jewell[a], Garreth Ruane[b], Stuart Shaklan[a], Dimitri Mawet[b], and DaveRedding[a]

[a]Jet Propulsion Laboratory, California Institute of Technology, 4800 Oak Grove Dr., Pasadena, CA 91109, USA;
[b]Department of Astronomy, California Institute of Technology, 1200 E. California Blvd., Pasadena, CA 91125, USA

ABSTRACT

The goal of directly imaging Earth-like planets in the habitable zone of other stars has motivated the design of coronagraphs for use with large segmented aperture space telescopes. In order to achieve an optimal trade-off between planet light throughput and diffracted starlight suppression, we consider coronagraphs comprised of a stage of phase control implemented with deformable mirrors (or other optical elements), pupil plane apodization masks (gray scale or complex valued), and focal plane masks (either amplitude only or complex-valued, including phase only such as the vector vortex coronagraph). The optimization of these optical elements, with the goal of achieving 10 or more orders of magnitude in the suppression of on-axis (starlight) diffracted light, represents a challenging non-convex optimization problem with a nonlinear dependence on control degrees of freedom. We develop a new algorithmic approach to the design optimization problem, which we call the "Auxiliary Field Optimization" (AFO) algorithm. The central idea of the algorithm is to embed the original optimization problem, for either phase or amplitude (apodization) in various planes of the coronagraph, into a problem containing additional degrees of freedom, specifically fictitious "auxiliary" electric fields which serve as targets to inform the variation of our phase or amplitude parameters leading to good feasible designs. We present the algorithm, discuss details of its numerical implementation, and prove convergence to local minima of the objective function (here taken to be the intensity of the on-axis source in a "dark hole" region in the science focal plane). Finally, we present results showing application of the algorithm to both unobscured off-axis and obscured on-axis segmented telescope aperture designs. The application of the AFO algorithm to the coronagraph design problem has produced solutions which are capable of directly imaging planets in the habitable zone, provided end-to-end telescope system stability requirements can be met. Ongoing work includes advances of the AFO algorithm reported here to design in additional robustness to a resolved star, and other phase or amplitude aberrations to be encountered in a real segmented aperture space telescope.

Keywords: vortex coronagraph, optimization, deformable mirrors, apodization

1. INTRODUCTION

The goal of directly imaging Earth-like planets in the habitable zone of other stars in our galaxy (0.7 to 1.5 AU from the host star) has motivated the design of coronagraphs for use with large segmented aperture space telescopes. A star 10, 30, or 50 parsec away hosting a planet at 1AU, will require a telescope approximately 3.4, 10.2, or 17.0 meters in diameter respectively to image (at a wavelength of 550 nm) the planet in a focal plane at 3 diffraction limited "resolution elements" (or 3 λ/D) from the on-axis star. Moreover, the star is 10 billion times brighter than the planet in reflected light.[1] The goal of direct imaging of exoplanets in the habitable zone therefore requires large aperture space telescopes, in order to collect enough photons from the planet, as well as some method of high-contrast imaging, in order to suppress the diffracted starlight even as close as an Inner Working Angles (IWA) of 3 λ/D. Therefore, achieving a direct imaging capability for exoplanets in the habitable zone requires the development of high-contrast imaging coronagraphs or starshades designed to work with large, segmented aperture, space telescopes.

Further author information: send correspondence to Jeffrey.B.Jewell@jpl.nasa.gov

Optimal coronagraph designs must strike a balance between planet light throughput and diffracted starlight suppression. We have excellent coronagraph designs for simple, uniform circular apertures, such as a monolithic primary with an off-axis secondary mirror. However, we currently do not have the technological means to increase telescope primary mirror diameters to the size driven by exoplanet imaging science goals with uniform circular apertures, necessitating new coronagraph designs capable of 10^{-10} suppression of diffracted starlight from the additional structure in segmented apertures.

The coronagraphs we will consider are composed of two stages of phase control (in two planes, implemented with deformable mirrors or other devices), a focal plane mask, and a Lyot stop. General end to end optimization of a coronagraph represents a non-convex problem with a nonlinear dependence on control parameters. In this paper, we introduce a new algorithmic approach to coronagraph optimization motivated by the intuition that we can find good coronagraph designs which best match the "input-output" of ideal coronagraphs for a given aperture. We will make this intuition more precise in what follows.

The results in this paper are with respect to optimization of either the two phase controls (DM's) with the focal plane fixed with a vortex phase only mask, and the Lyot plane fixed as a binary mask, typically either an annulus or slightly undersized aperture mask. We briefly comment on an application of the AFO algorithm adapted to apodization solutions tailored for use with a vortex focal plane mask - for a detailed discussion of these apodozation solutions and sensitivity analysis we refer the reader to G.Ruane et al, "Performance and Sensitivity of Vortex Coronagraphs on Segmented Space Telescopes", in these proceedings, as well as a summary of apodization solutions for a catalog of potential segmented aperture designs[2] We summarize application of the auxiliary field algorithm for the catalog of apertures in the Segmented Coroangaph Design and Analysis (SCDA) Program (led by Stuart Shaklan), as well as application to the LUVOIR initial aperture design.

2. THE CORONAGRAPH DESIGN OPTIMIZATION PROBLEM

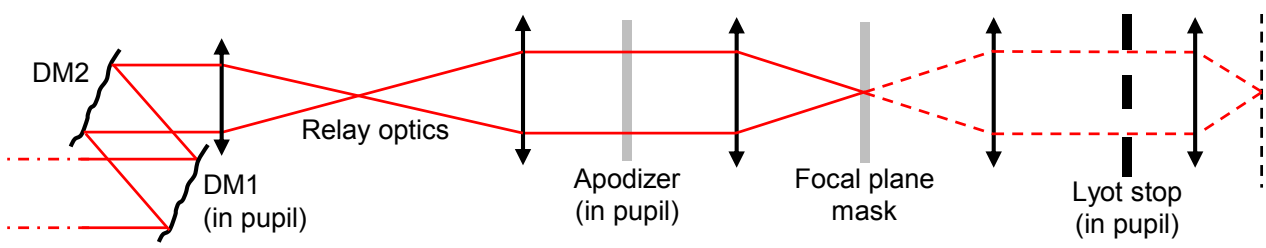

Figure 1. Coronagraph model and control degrees of freedom to be optimized for suppression of diffracted starlight.

In Fig. 1 we show a schematic of the coronagraph model used here. The model begins at an entrance pupil plane, where we have a deformable mirror for manipulation of the phase of the field. We then Fresnel propagate to another plane containing a second deformable mirror. We Fresnel propagate back to a conjugate pupil plane, after which we Fourier transform to a focal plane, where we have a mask (for this paper we use a vortex phase only mask). We then inverse Fourier transform to the Lyot plane where we use a binary Lyot stop, after which we Fourier transform the field to reach the final science focal plane. To fix notation, we represent the forward propagation of the entrance pupil electric field to the final science focal plane according to

$$\mathcal{E}(\xi) \quad = \quad \left(F\Theta F^{\dagger}\Omega F\right)\left(P_{\lambda}^{\dagger}e^{i\Gamma(\lambda_0/\lambda)}P_{\lambda}e^{i\Phi(\lambda_0/\lambda)}\right)X(\xi) \tag{1}$$

where the various optical elements are:

1. Entrance pupil electric field $X(\xi)$ (parametrized by the location ξ of the source in the focal plane). In this notation the on-axis source (i.e. the star) is $X(0)$, and assumed to be a re-imaged version of the telescope primary aperture in the coronagraph entrance pupil.

2. Entrance pupil phase control degrees of freedom (implemented by an optical element such as a deformable mirror) represented as $e^{i\Phi(\lambda_0/\lambda)}$. In this notation, we mean that the phase Φ has some value at every pixel in the entrance pupil, and $e^{i\Phi(\lambda_0/\lambda)}$ represents the complex-valued phase factor multiplying the incident electric field $X(\xi)$.

3. Fresnel propagation, denoted P_λ, from the entrance pupil to what we call the "Fresnel plane" for purposes of discussion in what follows.

4. Fresnel plane phase control degrees of freedom represented as $e^{i\Gamma(\lambda_0/\lambda)}$.

5. Fresnel propagation back to a reference conjugate pupil plane, denoted $P_\lambda^\dagger$.

6. Fourier transform, denoted F to a focal plane.

7. Multiplication of the incident field in the focal plane with a focal plane mask denoted Ω. For the purposes of this paper, we will fix Ω to be a vortex phase only focal plane mask $e^{il\phi}$, with ϕ the polar angle in cylindrical coordinates in the focal plane, and l the integer "topological chage".

8. Inverse Fourer transform to the Lyot (pupil) plane, with Lyot stop mask Θ.

9. A final Fourier transfrom to the science focal plane.

In the case of a uniform circular aperture, a vortex coronagraph with slightly undersized outer radius Lyot stop provides *perfect* suppression of an on-axis point source. As discussed earlier however, the drive to larger telescopes for exoplanet imaging requires segmented telescopes, resulting in diffraction from the additional structure of segment gaps and also the secondary mirror and support struts. This diffracted light makes the vortex unusable for segmented aperture telescopes - our problem then is to optimize either phase corrections in the entrance and Fresnel planes, and / or apodization in the conjugate pupil plane. The design optimization problem involves finding the phase or apodization resulting in $\sim 10^{-10}$ average contrast while allowing maximal planet light through. We now discuss a novel algorithm developed to solve this optimization problem, and show the resulting solutions enabling a vortex to work with large segmented aperture telescopes.

3. AUXILIARY FIELD ALGORITHM FOR CORONAGRAPH OPTIMIZATION

Coronagraph optimization is a non-convex optimization problem with a nonlinear dependence on parameters. The non-convex nature of the problem is due to the coronagraph architecture - we have control degrees of freedom in different planes, leading to the structure of a product of (a parametric family of) linear operators. The nonlinear nature of the problem is due to the fact that we use phase control, and so have a complex exponential dependence of the objective on our control degrees of freedom.

One approach to the minimization of $\|QCU(\Gamma,\Phi)X(0)\|^2$ is gradient descent and related approaches (conjugate gradient descent, or variable metric). These methods compute the direction resulting in a steep local decrease of the function, followed by a line search along this direction resulting in a minimum. However, the nonlinear dependence on phase degrees of freedom results in a computationally expensive line search. Other sub-optimal criteria might be used (for example a backtracking line search terminating based on the Armijo-Goldstein condition[3]). In addition to computationally expensive line searches, gradient descent techniques can result in local minima solutions, requiring other tricks to jump out and eventually settle on good coronagraph designs.

Another strategy for coronagraph optimization is to look for a way to introduce convex, linear sub-problems as a way of informing the optimization of the nonlinear degrees of freedom. Recent applications of stroke minimization Electric Field Conjugation (EFC)[4] are an example of this family of algorithm. This method introduces a *linear approximation of the nonlinear phase control on an incident field directly in the objective function*, and then solves for the optimal phase variation (a function of a regularization parameter controlling the amplitude of variation). The approximation, for small phase variations

$$e^{iH(a+da)} \approx e^{iHa}\,(1+iHda) \tag{2}$$

leads to a linearized form for the perturbation to the focal plane electric field

$$\mathcal{E} \approx \mathcal{E}_0 + Sda \tag{3}$$

where S is the "sensitivity matrix" (the local Jacobian of the focal plane field with respect to the phase control degrees of freedom in either the entrance pupil plane or Fresnel plane). Substituting this approximation into the objective function leads to the linear subproblem

$$\begin{aligned} \hat{\delta} &= \min_{\delta} \left(\|\mathcal{E}_0 + S\delta\|^2 + \mu\|\delta\|^2 \right) \\ &= \left(\mu I + S^\dagger S\right)^{-1} (-1) S^\dagger \mathcal{E}_0 \end{aligned} \tag{4}$$

The complication with the above is that for coronagraph optimization with segmented apertures, the *dynamic range of contrast we need to suppress requires DM variations that are well outside the validity of the linear approximation above*. We are therefore forced to recompute the sensitivity matrix S about the current DM solutions frequently as we optimize.[5]

Given the computational expense for both gradient descent line searches and recomputing the Jacobian for the focal plane field with respect to phase degrees of freedom, we look for alternative algorithms utilizing convex linear subproblems informing the variations of nonlinear control degrees of freedom. We begin with the question: *"What (conjugate pupil) field would result in vanishing energy in the dark hole region?"* It is interesting to consider such a set of conjugate pupil fields since the field in the Fresnel or entrance pupil can then be immediately computed within our model by propagating "backwards" (possible since the Fresnel propagators are invertible; in fact *unitary* operators with an inverse given by their adjoint). This would suggest that adjusting the phase control degrees of freedom can be done almost analytically given a specific target field propagated back from the conjugate pupil. We note that such an approach is similar in spirit to the "Active Compensation of Aperture Discontinuities" (ACAD) approach, where the DM's were adjusted to achieve a nearly uniform field in a circular region in the conjugate pupil. However, our approach is not to assume a specific target conjugate pupil field, *but rather ask the coronagraph itself which field would result in vanishing energy in the dark hole region.*

Of course, there are many possible conjugate pupil fields which give vanishing energy from the on-axis source in the dark hole region. We immediately recognize the need to regularize our choice. One obvious regularization is to penalize the conjugate pupil field from being too far away from the actual physical field incident on the conjugate pupil. If we begin with flat DM's (no phase wavefront control), we have a one dimensional parametric family of conjugate pupil plane fields, depending on a parameter "b", striking a balance between vanishing dark hole energy for the on-axis source and not deviating too far from the actual physical conjugate field,

$$\hat{W} = \min_{W} \left(\|QCW\|^2 + b\,\|W - A\|^2 \right) \tag{5}$$

(with the entrance pupil aperture mask A set by the telescope design). The solution to this problem is

$$\hat{W} = \left(bI + C^\dagger QC\right)^{-1} bA \tag{6}$$

(where $C^\dagger$ is the conjugate transpose of the coronagraph operator C), and represent a one-parameter family of target fields depending on the regularization parameter 'b'. We will discuss details of solving this (linear) problem in what follows, as well as prove that the target field, in the limit $\lim_{b\to 0}$, has *vanishing energy in the dark hole region* We show such an example target field in Fig. 2, computed for a four ring hexagonal segmented aperture telescope (specifically the LUVOIR mission concept architecture 'A' telescope design), with a charge 6 vortex focal plane mask and a simple annular Lyot stop downstream of the conjugate pupil.

As this fictitious conjugate pupil field W has vanishing dark hole energy, it is an ideal target to try to "hit" by adjusting our phase control degrees of freedom. We do so by next solving for the phase degrees of freedom which best approximate W,

$$\{\Gamma, \Phi\} = \min_{\Gamma,\Phi} \left(\left\| W - \left(P_\lambda^\dagger e^{i(\lambda_0/\lambda)\Gamma} P_\lambda e^{i(\lambda_0/\lambda)\Phi} \right) A \right\|^2 \right) \tag{7}$$

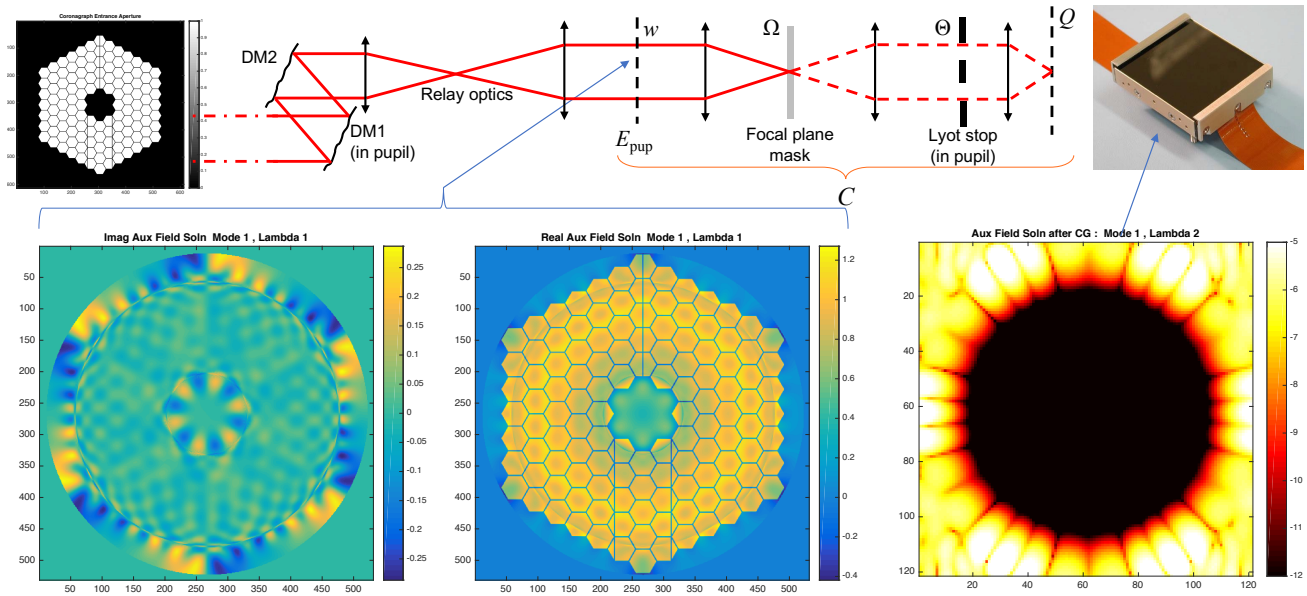

Figure 2. The imaginary (lower left) and real (lower middle) parts of the target (conjugate plane) complex electric field for the on-axis source has $\lim_{b\to 0} \|QCW\|^2 = 0$ energy in the dark hole region where planets live!

While this is a nonlinear, non-convex optimization subproblem, the unitary (and invertible) nature of the Fresnel propagators, and phase control in the Fresnel plane itself, allow accurate, and efficient, solutions to this subproblem by alternating minimization of one DM with the other fixed, and back-propagating the target field to the plane being optimized (details to be discussed in what follows).

Our new algorithmic approach is to simply iterate these two steps, where given our current DM phase control solution we solve for the target field W, and with that ideal conjugate pupil field, we adjust the DM's to best approximate that target. In what follows we will refer to this algorithm as the "Auxiliary Field Optimization" (AFO) algorithm (the name referring to the embedding of the original optimization problem for the phase control degrees of freedom into a larger dimensional problem including the fictitious target conjugate pupil plane field W as "auxiliary variables" to help inform the choice of phase variations).

It is possible to show that this algorithm, based on the above simple intuition, can be *proven to converge to a local minimum of our objective* (as discussed in detail in Appendix D). "Under the hood", the algorithm is a variant of an "expectation-maximization" algorithm,[6] and hints at the value of a probabilistic setting for constructing coronagraph design optimization algorithms. It is beyond the scope of this paper to explore probabilistic or random search ideas further, but we note simply that such algorithms (such as simulated annealing) are among the few capable of delivering *global optimal solutions* to non-convex problems, although at potentially tremendous computational expense. We simply use a probabilistic framework here to formulate a simpler, deterministic algorithm (capable of only "local minimum" guarantees). We now proceed to discuss the numerical implementation of the algorithm and then show results on various segmented aperture telescope designs.

4. NUMERICAL IMPLEMENTATION OF THE AUXILIARY FIELD ALGORITHM

4.1 Solving for the Target Field

As noted above, the first step of an iterative cycle of the AFO is to solve for an updated target conjugate pupil field

$$\begin{aligned} \hat{W} &= \min_{W} \left(\|QCW\|^2 + b \left\| \hat{W} - U(\Gamma,\Phi)A \right\|^2 \right) \\ &= \left(bI + C^\dagger QC \right)^{-1} bU(\Gamma,\Phi)A \end{aligned} \tag{8}$$

While this is a linear problem, it is non-trivial to solve. For numerical accuracy, it is common to use ~ 1000, or ~ 2000 pixels across the entrance pupil aperture, and further zero pad to give sufficient sampling in subsequent focal planes in the coronagraph. As we have identified the conjugate pupil as a convenient place to solve for an ideal field, the matrix to be inverted $\left(bI + C^\dagger QC\right)^{-1}$ is $\sim 10^6 \times 10^6$ even if restricted to a region in the conjugate pupil matched to the support of the entrance pupil. A matrix of this size is prohibitive to store let alone compute by brute force and invert.

However, we recall the "Sherman-Woodbury" matrix identity for the inverse of this matrix,

$$\left(bI + C^\dagger QC\right)^{-1} = \left[I - C^\dagger Q \left(bI + QCC^\dagger Q\right)^{-1} QC\right] \tag{9}$$

The significance of this identity is two-fold: 1) we can *multiply* by the "forward" and "adjoint" coronagraph operators using forward and inverse Fourier transforms and multiplication by the vortex focal plane (or its complex conjugate) respectively, and 2) the "internal" matrix $\left(bI + QCC^\dagger Q\right)^{-1}$ is of a size $N_{DH} \times N_{DH}$, with N_{DH} the number of pixels in the science focal plane dark hole region. *This is a much smaller matrix, typically* $10^4 \times 10^4$ *for focal plane sampling of* 4 *pixels*/(λ/D)*, and inner and outer working angles of* 3 λ/D *and* 10 λ/D *respectively.*

Our solution for the auxiliary field, using the matrix identity above is therefore

$$\hat{W} = \left[I - C^\dagger Q \left(bI + QCC^\dagger Q\right)^{-1} QC\right] \left(P^\dagger e^{i\Gamma} P e^{i\Phi} A\right) \tag{10}$$

We proceed to solve this by

1. Compute the true conjugate pupil field for entrance pupil aperture A

$$Y_1 = P^\dagger e^{i\Gamma} P e^{i\Phi} A \tag{11}$$

   (using Fresnel propagation and operating with the current DM phase solutions).

2. Send the conjugate pupil field through the coronagraph (through the vortex and Lyot stop to the science focal plane), by computing

$$Y_2 = \left(F\Theta F^\dagger \Omega F\right) Y_1 \tag{12}$$

   (with F and $F^\dagger$ forward and inverse Fourier transforms respectively, Ω the phase only vortex focal plane mask, and Θ the Lyot stop).

3. Keep only the forward field in the dark hole region by multiplying by the binary dark hole region mask $Y_3 = QY_2$.

4. Solve the linear problem restricted to the dark hole region,

$$Y_4 = \left(bI + QCC^\dagger Q\right)^{-1} Y_3 \tag{13}$$

5. Operate with the *adjoint coronagraph operator* (a linear mapping from the science focal plane to the conjugate pupil plane),

$$Y_5 = \left(F^\dagger \Omega^* F \Theta^* F^\dagger\right) Y_4 \tag{14}$$

   (where Ω^* and Θ^* are the complex conjugates of the vortex focal plane and Lyot stop masks respectively).

6. Subtract from the true conjugate pupil field the correction Y_4 to solve for the new target auxiliary field

$$\hat{W} = \left(P^\dagger e^{i\Gamma} P e^{i\Phi} A\right) - Y_5 \tag{15}$$

We refer to Equation 13 above as the "internal AFO linear problem", and we solve this by brute force having precomputed and stored a singular value decomposition of the matrix $QCC^\dagger Q \equiv U\ \mathrm{Diag}(S)\ U^\dagger$, with the columns of U the eigenmodes of the matrix $QCC^\dagger Q$. We discuss the details of the computation of this matrix and associated eigenmdoes in Appendix A.

We now stress the physical importance of the eigenmodes of the internal AFO matrix used in explicitly solving Eequation 13 above, and show that the auxiliary field W in the limit of very small regularization parameter $b \ll 1$ gives vanishing energy in the dark hole. To review, the eigenmodes satisfy the linear equation

$$QCC^\dagger Q|f_j\rangle = |\alpha_j|^2|f_j\rangle \tag{16}$$

where the eigenvalues are deliberately written as the modulus squared of a complex number $|\alpha_j|^2 = \alpha_j^*\alpha_j$ for reasons which will become clear. In the above we are borrowing a notation inherited from Quantum Mechanics to efficiently keep track of generally complex eigenmodes, where $|f_j\rangle$ can abstractly be thought of as a (complex valued) "column vector" and $\langle f_j|$ be thought of as a "row vector". The notation is also convenient as it denotes the eigenmodes as "vectors" in a Hilbert space of functions without explicit reference to basis. While working numerically, we will represent these modes at each "pixel" of the plane in which these modes live, i.e. focal plane or pupil plane. (**ref**). The eigenmodes form an orthogonal basis set, which means the inner products satisfy

$$\langle f_j|f_k\rangle = \begin{array}{ll} 1 & \text{for } j = k \\ 0 & \text{otherwise} \end{array} \tag{17}$$

We emphasize that the eigenmodes $|f_j\rangle$ have support in the dark region (they vanish completely outside the dark hole). We consider, for each focal plane dark hole eigenmode, as associated *pupil plane mode*

$$C^\dagger Q|f_j\rangle = \alpha_j|g_j\rangle \tag{18}$$

We investigate the properties of these pupil plane modes. First we compute the inner product of any two of these modes, and find they are *orthogonal*

$$\begin{aligned} \alpha_j^*\alpha_k\langle g_j|g_k\rangle &= \langle C^\dagger Q f_j|C^\dagger Q f_k\rangle \\ &= \langle f_j|(C^\dagger Q)^\dagger C^\dagger Q|f_k\rangle \\ &= \langle f_j|QCC^\dagger Q|f_k\rangle \\ &= |\alpha_k|^2\langle f_j|f_k\rangle \\ &= |\alpha_k|^2\delta_{jk} \end{aligned} \tag{19}$$

This shows that $\langle g_j|g_k\rangle = \delta_{jk}$, and the associated pupil plane modes $|g_j\rangle$ form an *orthogonal basis for pupil plane modes which directly contribute energy to the dark hole region.* Finally we can show that the pupil plane modes also generate the original focal plane eigenmodes. Operating on both sides of the defining equation for the pupil plane modes 18 with QC we have

$$\begin{aligned} QC\left(C^\dagger Q|f_j\rangle\right) &= \alpha_j(QC)|g_j\rangle \\ &= \alpha_j^*\alpha_j|f_j\rangle \end{aligned} \tag{20}$$

or simply that

$$QC|g_j\rangle = \alpha_j^*|f_j\rangle \tag{21}$$

This shows that the entire action of the vortex and Lyot stop in mapping a conjugate pupil field to the dark hole region can be compactly written in terms of the "input-output" response,

$$QC = \sum_j \alpha_k^*\ |f_j\rangle\langle g_j| \tag{22}$$

while the *adjoint* linear operator mapping the dark hole region to an associated conjugate pupil plane is given by

$$C^\dagger Q \quad = \quad \sum_k \alpha_k \; |g_k\rangle\langle f_k| \tag{23}$$

and of course, with this "factorization" we recover our original eigenmode representation

$$\begin{aligned} QCC^\dagger Q &= \left(\sum_j \alpha_j^* \; |f_j\rangle\langle g_j|\right)\left(\sum_k \alpha_k \; |g_k\rangle\langle f_k|\right) \\ &= \sum_{jk} \alpha_j^* \alpha_k \; |f_j\rangle \; \langle g_j|g_k\rangle \; \langle f_k| \\ &= \sum_j |\alpha_j|^2 \; |f_j\rangle\langle f_k| \end{aligned} \tag{24}$$

(where in the last line we used the orthogonality relation $\langle g_j|g_k\rangle = \delta_{jk}$).

When viewed in terms of this eigenmode decomposition of the linear mapping from conjugate to science focal plane, one quickly sees that our implicit goal for the phase control is to somehow *orthogonalize* the on-axis source in the entrance pupil from the set of dark hole conjugate pupil eigenmodes. The significance of the auxiliary field is that, in the limit of vanishing regularization $b \ll 1$, it is *exactly* a projection of the on-axis source into the null space of QC, giving zero energy in the dark hole, since we can show the solution is given in terms of the eigenmodes $|g_j\rangle$

$$|\hat{W}\rangle \quad = \quad |U(\Gamma,\Phi)A\rangle - \left(\sum_j |g_j\rangle \left(\frac{|\alpha_j|^2}{b+|\alpha_j|^2}\right) \langle g_j|U(\Gamma,\Phi)A\rangle\right) \tag{25}$$

As $b \to 0$, the above perfectly vanishes for all the pupil modes $|g_j\rangle$ that map to the focal plane dark hole (once passed through the coronagraph C). We remind the reader of Figure 2, showing exactly this property.

4.2 Variation of Phase

We now discuss the second step of the AFO iteration, in which we adjust the DM phase solutions to best match the updated auxiliary field W (itself a function of the previous DM solution estimate). With the updated auxiliary field in hand, we want to minimize the approximation error between the true conjugate pupil field and the target by solving Equation 7. This is still a hard problem as it is a non-convex subproblem with a nonlinear dependence on parameters. For this step, we alternate a minimization of one DM with the other fixed, which results at least in a reduction of approximation error.

We make the choice to first optimize the entrance pupil phase Φ given the target auxiliary field while holding the Fresnel plane DM phase Γ fixed, i.e. we want to solve

$$\delta\Phi \quad = \quad \min_{\delta\Phi}\left(\int d\lambda \; \left\|W_\lambda - P_\lambda^\dagger e^{i\Gamma\;(\lambda_0/\lambda)} P_\lambda e^{i\Phi(\lambda_0/\lambda)} e^{i\delta\Phi(\lambda_0/\lambda)} \; A\right\|^2\right) \tag{26}$$

It is here that we appreciate one of the motivations for solving for the auxiliary field in the conjugate pupil plane - we can take advantage of the *unitary* nature of the Fresnel propagators, giving their inverse simply as their conjugate transpose (or adjoint), $P^{-1} = P^\dagger$,. The adjoint of the Fresnel propagator is easily shown to be the Fresnel propagator with a reversed sign of the distance of propagation along the optical axis. This allows us to back-propagate the target auxiliary field to either the Fresnel plane or entrance pupil plane, where we can almost analytically find the variation in phase required to hit the back-propagated target.

To make this explicit in solving the entrance pupil phase variation in Equation 26, we form the back-propagated entrance pupil target auxiliary field

$$Z_\lambda(\Gamma) = e^{-i\Phi(\lambda_0/\lambda)} P_\lambda^\dagger e^{-i\Gamma\;(\lambda_0/\lambda)} P_\lambda W \tag{27}$$

Because our approximation error metric is chosen with respect to the *inner-product norm*, unitary operators can be absorbed and we have exactly

$$\begin{aligned}\delta\Phi &= \min_{\delta\Phi}\left(\int d\lambda\ \left\|W_\lambda - P_\lambda^\dagger e^{i\Gamma\ (\lambda_0/\lambda)} P_\lambda e^{i\Phi(\lambda_0/\lambda)} e^{i\delta\Phi(\lambda_0/\lambda)}\ A\right\|^2\right) \\ &= \min_{\delta\Phi}\left[\int d\lambda\ \left(Z_\lambda^*(\Gamma) - e^{-i\delta\Phi(\lambda_0/\lambda)}\ A^*\right)\left(Z_\lambda(\Gamma) - e^{i\delta\Phi(\lambda_0/\lambda)}\ A\right)\right] \end{aligned} \tag{28}$$

A variation in $\delta\Phi$ leads to the condition

$$0 = \int d\lambda\ \left(\frac{\lambda_0}{\lambda}\right)\left(Z_\lambda(\Gamma)e^{-i\delta\Phi(\lambda_0/\lambda)}A^* - Z_\lambda^*(\Gamma)e^{i\delta\Phi(\lambda_0/\lambda)}A\right) \tag{29}$$

We define the modulus and phase at each wavelength

$$Z_\lambda(\Gamma)A^* \equiv |Z_\lambda(\Gamma)A^*|\ e^{i\Psi_\lambda} \tag{30}$$

so that the phase variation minimum satisfies

$$\begin{aligned} 0 &= \int d\lambda\ \left(\frac{\lambda_0}{\lambda}\right)\ |Z_\lambda(\Gamma)A^*|\ \left(e^{+i(\Psi_\lambda - \delta\Phi(\lambda_0/\lambda))} - e^{-i(\Psi_\lambda - \delta\Phi(\lambda_0/\lambda))}\right) \\ &= 2i\int d\lambda\ \left(\frac{\lambda_0}{\lambda}\right)\ |Z_\lambda(\Gamma)A^*|\ \left(\frac{e^{+i(\Psi_\lambda - \delta\Phi(\lambda_0/\lambda))} - e^{-i(\Psi_\lambda - \delta\Phi(\lambda_0/\lambda))}}{2i}\right) \\ &= 2i\int d\lambda\ \left(\frac{\lambda_0}{\lambda}\right)\ |Z_\lambda(\Gamma)A^*|\ \ \sin\left[\Psi_\lambda - \delta\Phi(\lambda_0/\lambda)\right] \end{aligned} \tag{31}$$

Notice that for single wavelengths, we set the update in $\delta\Phi$ to Ψ_λ, which makes any monochromatic form above vanish. However, for any finite bandpass we only have the one DM or phase screen surface to minimize the above. Assuming the validity of a small angle approximation $\sin x \approx x$, we solve for an approximate phase variation

$$\begin{aligned} 0 &= \int d\lambda\ \left(\frac{\lambda_0}{\lambda}\right)\ |Z_\lambda(\Gamma)A|\ \sin\left[\Psi_\lambda - \delta\Phi(\lambda_0/\lambda)\right] \\ &\approx \int d\lambda\ \left(\frac{\lambda_0}{\lambda}\right)\ |Z_\lambda(\Gamma)A|\ \left[\Psi_\lambda - \delta\Phi(\lambda_0/\lambda)\right] \end{aligned} \tag{32}$$

giving the update to the phase

$$\delta\Phi = \frac{\int d\lambda\ \left(\frac{\lambda_0}{\lambda}\right)\ |Z_\lambda(\Gamma)A|\,\Psi_\lambda}{\int d\lambda\ \left(\frac{\lambda_0}{\lambda}\right)^2\ |Z_\lambda(\Gamma)A|} \tag{33}$$

The same procedure is then applied to solve for a variation in the DM in the Fresnel plane with the new entrance pupil phase $\Phi + \delta\Phi$ fixed.

We comment on the use of the small angle approximation above in Equation 32. This is *not* the same as a linearization of the DM action on an incident field. It assumes that the resulting approximation error (due to the fact that our DM has an assumed optical path difference wavelength dependence) to the ideal wavelength dependent phase variation Ψ_λ is small. This is clearly the case for small enough band. In practice we have found this approximate method of updating the phase to work well for 10% bandwidths. We emphasize here that future refinements of the AFO algorithm can include more sophisticated solutions to the phase optimization subproblem (eqn. 26), possibly including gradient descent or other iterative approach, while taking advantage of the fast back-propagation of the target field in equation 27.

We note that while we could compute several cycles of phase variation above, we have found that in practice one cycle followed by another update in the target auxiliary field suffices to give convergence to phase solutions capable of 10^{-10} contrast levels over 10% bandwidths. Finally, we refer the reader to Appendix B for a generalization of the phase updates above when solving explicitly for coefficients in some set of DM "influence functions".

5. APPLICATION TO THE SCDA AND LUVOIR APERTURES

We have applied the AFO algorithm to a variety of potential segmented telescope aperture designs considered in the Segmented Coronagraph Design and Analysis (SCDA) study (led by Stuart Shaklan of the NASA Jet Propulsion Laboratory). Examples of possible segmented apertures considered at shown in Figure 3. The AFO algorithm resulted in both beam-shaping and apodization solutions using a vortex focal plane mask and simple Lyot stop, with 10^{-10} on-axis source diffracted light suppression, with excellent throughput. We now show in detail the contrast and throughout for both an off-axis, unobscured segmented aperture, as well as well as for the LUVOIR architecture 'A' design.

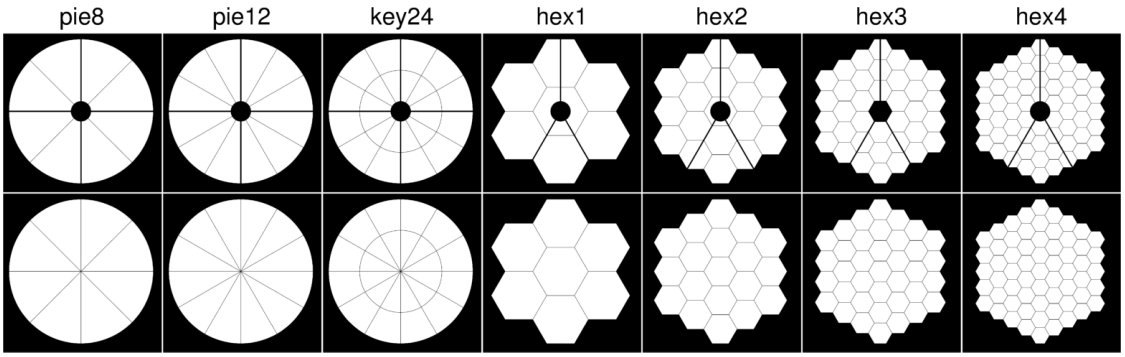

Figure 3. Segmented Coronagraph Design and Analysis (SCDA) study, led by Stuart Shaklan (JPL), supported by the Exoplanet Exploration Program (ExEP).

5.1 Unobstructed Apertures

In Figures 4 and 5, we show the resulting solutions for beam shaping to an unobstructed four-ring Hex aperture. A charge 6 vortex focal plane mask was used with a simple uniform circular Lyot stop with an outer radius 0.99 with respect to the outer radius of the entrance pupil aperture. A DM array with actuator pitch of 400×10^{-6} meters was used in the model, with localized DM influence functions. The DM solutions were optimized over a 10% band to suppress an on-axis point source.

5.2 AFO Algorithm Solution for the LUVOIR 'A" Aperture

In Figures 6 and 7, we show the resulting beam-shaping solutions for an "ideal DM" for the LUVOIR architecture 'A' aperture. The "ideal DM" solutions are modeled as Optical Path Difference (OPD) phase masks in both the entrance pupil and Fresnel Plane. The entrance aperture was left unmodified (i.e. the outer perimeter of the aperture was not masked out with a smaller circular mask), and the Lyot stop (shown in the lower left of Figure 7) was a copy of the entrance pupil aperture with a circular mask covering the secondary mirror. *No apodization was used* in the optimization, with the 10^{-10} (normalized) contrast achieved purely with the phase solutions in the entrance and Fresnel planes. *We emphasize that these coronagraph design solutions are for an on-axis point source.* These solutions are a preliminary study of the feasibility of a vortex focal plane mask with a central obscured aperture such as that considered for the LUVOIR 'A" architecture. Work in progress is including robustness to the finite size of the star in the optimization, which must be taken into account for a primary mirror of 15 meters used for the LUVOIR mission concept.

We note that the use of "ideal DM's" here for LUVOIR is significant in demonstrating the potential throughput gains if the on-axis diffracted light is suppressed with pure phase beam shaping. One of the unique capabilities of the AFO algorithm is the ability to solve for phase variations at each "pixel", leading to a solutions of prohibitive dimension for algorithms such as stroke minimization EFC (relying on computation of the Jacobian for each DM degree of freedom as outlined in[4]).

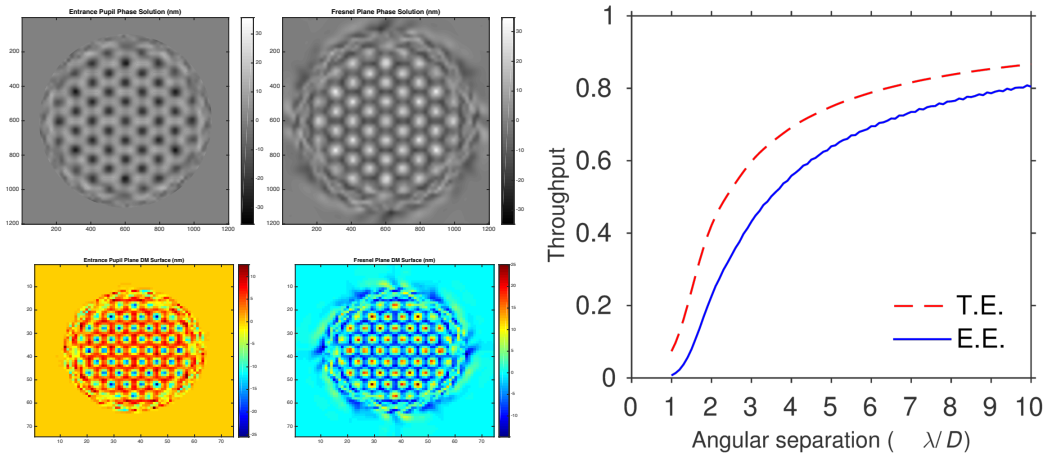

Figure 4. Deformable Mirror solutions for an unobstructed hex aperture. Upper left and right show the resulting phase applied on the Entrance Pupil and Fresnel Plane Deformable Mirror respectively, while the lower left and right show the actuator heights in nanometers. Plot (far right) shows that relative throughput as a function of angular separation for an off-axis source.

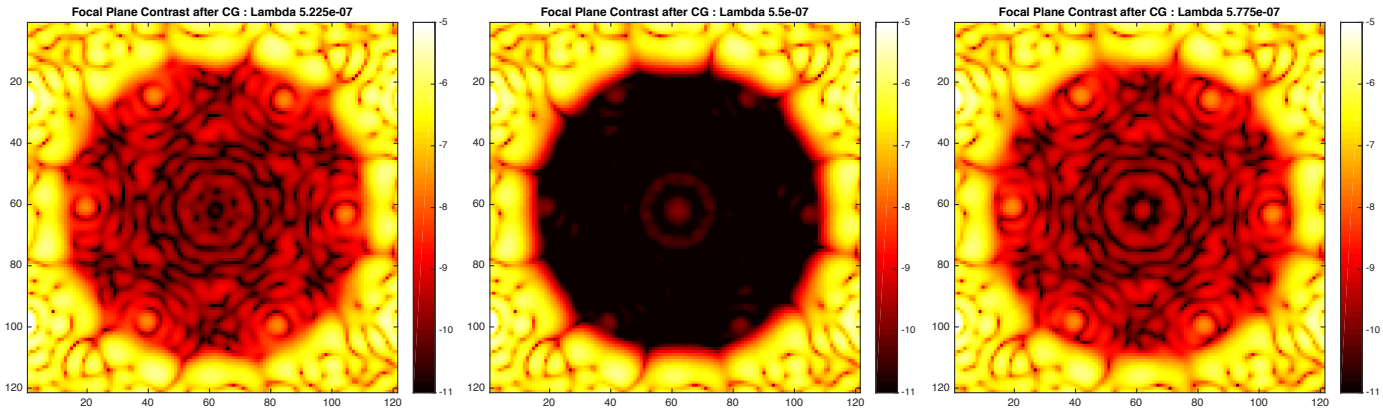

Figure 5. Science focal plane normalized intensity contrast for the DM solutions in Figure 4, at 522.5, 550, and 577.5 nanometers spanning a 10% bandpass. Bandpass averaged contrast achieved is 2.8×10^{-10}.

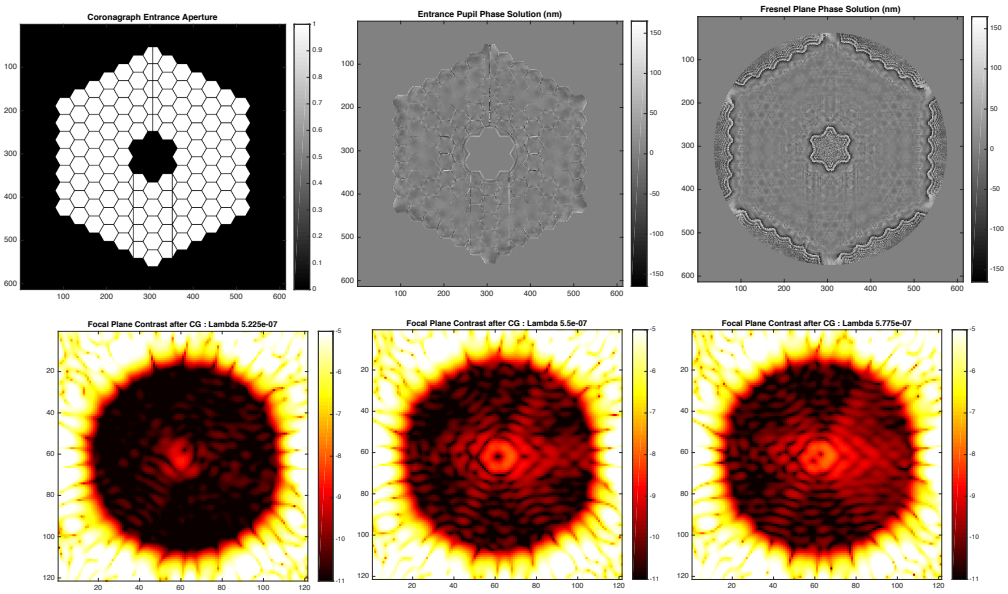

Figure 6. "Ideal DM" solutions for the LUVOIR "A" architecture, achieving 10^{-10} suppression in a 10% band (550 nm central wavelength) of diffracted light for an on-axis point source.

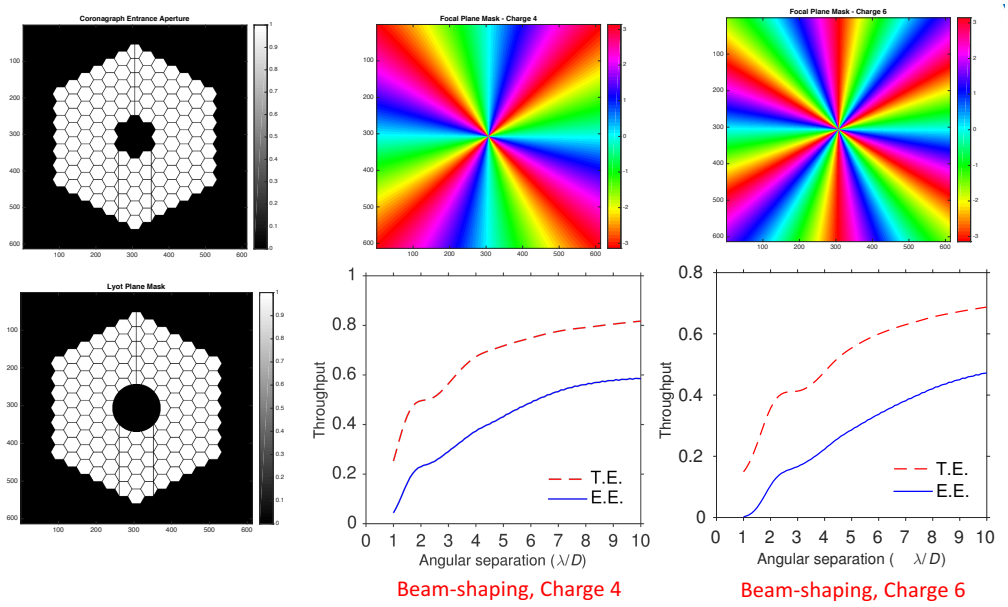

Figure 7. Comparison of relative throughput for "ideal DM" solutions for the LUVOIR "A" architecture, for a charge 4 and 6 vortex focal plane mask. Both solutions are designed to achieve 10^{-10} suppression in a 10% band (550 nm central wavelength) of diffracted light for an on-axis point source.

6. SUMMARY AND CONCLUSIONS

In summary, the goal of direct imaging of exoplanets in the habitable zone requires large (and therefore segmented) aperture telescopes together with some means of high-contrast imaging. We have developed a new "Auxiliary Field Optimization" (AFO) algorithm for coronagraph design for use with segmented apertures. Our initial focus in the development of the AFO algorithm has been to solve for either beam-shaping phase solutions (this paper), or apodization solutions[2] (see also G. Ruane et. al., these proceedings) for a fixed focal plane mask and Lyot stop. Motivated by the excellent performance of the vortex focal plane mask for unobscured uniform circular aperture telescopes, we have applied the AFO algorithm to find solutions enabling the vortex coronagraph to be used with segmented aperture telescopes. We find viable solutions for the catalog of *unobscured* SCDA apertures (either beam shaping or apodization) which are insensitive to diffraction from a resolved stellar disc of 0.1 mas (we refer again to G. Ruane et. al. for a detailed sensitivity analysis). For the *centrally obscured segmented apertures*, we find sensitivity to the resolved stellar disc when solutions are optimized for suppression of a point on-axis source alone. We are currently working to build into the optimization the ability to suppress a resolved stellar disc with a generalization of the AFO algorithm to include optimization over the focal plane mask, conjugate pupil complex (or gray-scale amplitude only) mask, along with phase beam shaping with two DM's.

The AFO algorithm used for solving for the "ideal DM" solutions is also of interest in considering potential technology development in order to boost coronagraph performance. Novel devices such as Liquid Crystal Polymers are now being developed that show the "ideal DM" solutions might be realizable in hardware. These solutions are also valuable in providing insight into the spatial frequencies needed for pure phase beam-shaping solutions, and shed light into the potential trade-offs of conjugate plane apodization and beam-shaping. The former reduces throughput but is achromatic, while the latter results in higher throughput albeit over a restricted wavelength bandpass. Which design is best suited to a given mission concept requires detailed sensitivity analysis and end-to-end simulation including wavefront estimation and control, as closed-loop control (implemted with DM's) will introduce a wavelength dependence and limit the bandpass over which we can achieve reasonable signal to noise (balancing both contrast and planet throughput).

APPENDIX A. COMPUTATION OF THE INTERNAL AUXILIARY FIELD MATRIX

Noting that there are eigenmodes such that

$$\begin{aligned} QCRR^\dagger C^\dagger Q|\phi_j\rangle &= |\beta_j|^2|\phi_j\rangle \\ R^\dagger C^\dagger Q|\phi_j\rangle &= \beta_j|f_j\rangle \\ QCR|f_j\rangle &= \beta_j^*|\phi_j\rangle \\ R^\dagger C^\dagger |Q|^2 CR|f_j\rangle &= |\beta_j|^2|f_j\rangle \end{aligned} \tag{34}$$

we have the identity

$$\begin{aligned} \tilde{\mathcal{O}} &= bX(0)U^\dagger \left[R^\dagger C^\dagger Q\left(bI + QCRR^\dagger C^\dagger Q\right)^{-1} QCR\right] UX(0) \\ &= X(0)U^\dagger \left(R^\dagger C^\dagger Q\left[\sum_j |\phi_j\rangle \left(\frac{b}{b+|\beta_j|^2}\right)\langle\phi_j|\right] QCR\right) UX(0) \\ &= bX(0)U^\dagger \left[\sum_j |f_j\rangle \left(\frac{|\beta_j|^2}{b+|\beta_j|^2}\right)\langle f_j|\right] UX(0) \end{aligned} \tag{35}$$

APPENDIX B. OPTIMIZATION OF DEFORMABLE MIRROR INFLUENCE FUNCTION ACTUATOR HEIGHTS

We now add details to the above if optimizing DM actuator heights, with the associated DM surface given by the influence functions,

$$\begin{aligned} \Gamma &= 4\pi\lambda_0^{-1} \sum_k h_k(p)\ d_k \\ \Phi &= 4\pi\lambda_0^{-1} \sum_k h_k(p)\ c_k \end{aligned} \tag{36}$$

where $\{c_k, d_k\}$ are the actuator heights (in physical units) and $h_k(p)$ is the k-th influence function (at pixel p). In matrix form then

$$\begin{aligned} \Gamma &= Hd \\ \Phi &= Hc \end{aligned} \tag{37}$$

where we absorb the $4\pi\lambda_0^{-1}$ in the columns of H.

As before we want to solve

$$\begin{aligned} \delta c &= \min_{\delta c} \left(\int d\lambda\ \left\| W_\lambda - P_\lambda^\dagger e^{i(\lambda_0/\lambda)\Gamma} P_\lambda e^{i(\lambda_0/\lambda)\Phi} e^{i(\lambda_0/\lambda)H\delta c}\ A \right\|^2 \right) \\ &= \min_{\delta\Phi} \left(\int d\lambda\ \left\| \left(e^{-i\Phi(\lambda_0/\lambda)} P_\lambda^\dagger e^{-i\Gamma\ (\lambda_0/\lambda)} P_\lambda W_\lambda \right) - e^{i(\lambda_0/\lambda)H\delta c}\ A \right\|^2 \right) \end{aligned} \tag{38}$$

(where for notational convenience we only explicitly referred to the DM actuator variations being considered, and Φ and Γ are determined by the current DM actuator settings as above).

As before we again define

$$Z_\lambda(\Gamma) = e^{-i\Phi(\lambda_0/\lambda)} P_\lambda^\dagger e^{-i\Gamma\ (\lambda_0/\lambda)} P_\lambda W \tag{39}$$

so that our minimization problem reduces to

$$\delta\Phi = \min_{\delta\Phi} \left[\int d\lambda\ \left(Z_\lambda^*(\Gamma) - e^{-i(\lambda_0/\lambda)H\delta c}\ A^* \right) \left(Z_\lambda(\Gamma) - e^{i(\lambda_0/\lambda)H\delta c}\ A \right) \right] \tag{40}$$

Setting the variation of the quadratic form above with respect to the actuator heights δc to zero (i.e. taking the gradient of the above with respect to δc and setting to 0) leads to the condition

$$0 = H^T \cdot \int d\lambda\ \left(\frac{\lambda_0}{\lambda} \right) \left(Z_\lambda(\Gamma) e^{-i(\lambda_0/\lambda)H\delta c} A^* - Z_\lambda^*(\Gamma) e^{i(\lambda_0/\lambda)H\delta c} A \right) \tag{41}$$

(where H^T is the transpose of the DM basis function response matrix). As before, we define the modulus and phase at each wavelength

$$Z_\lambda(\Gamma) A^* \equiv |Z_\lambda(\Gamma) A^*|\ e^{i\Psi_\lambda} \tag{42}$$

Therefore, the optimal DM variation satisfies

$$\begin{aligned} 0 &= H^T \cdot \int d\lambda\ \left(\frac{\lambda_0}{\lambda} \right)\ |Z_\lambda(\Gamma) A^*| \left(e^{i\Psi_\lambda} e^{-i(\lambda_0/\lambda)H\delta c} - e^{-i\Psi_\lambda} e^{i(\lambda_0/\lambda)H\delta c} \right) \\ &= (2i)\ H^T \cdot \int d\lambda\ \left(\frac{\lambda_0}{\lambda} \right)\ |Z_\lambda(\Gamma) A^*| \sin\left[\Psi_\lambda - (\lambda_0/\lambda) H\delta c \right] \\ &\approx (2i)\ H^T \cdot \int d\lambda\ \left(\frac{\lambda_0}{\lambda} \right)\ |Z_\lambda(\Gamma) A^*| \left(\Psi_\lambda - (\lambda_0/\lambda) H\delta c \right) \end{aligned} \tag{43}$$

(where in the last line we again approximate $\sin(x) \approx x$). The above gives a linear relation between the DM variations and a amplitude modulated source term from the Ψ_λ (*note - a slightly different form can be derived by first writing the objective to second order in the δc and including stroke minimization*).

Finally note the intuitive but *sub-optimal* approximate solution for the monochromatic case

$$\delta c = (H^T H)^{-1} H^T \Psi \tag{44}$$

This approximation *neglects the amplitude modulation from the* $|ZA^*|$ and should be corrected to

$$\delta c = \left(H^T |ZA^*| H\right)^{-1} H^T |ZA^*| \Psi \tag{45}$$

APPENDIX C. CONVERGENCE IN MEASURE

For solving for phase solutions, we want to minimize

$$\mathcal{O}(\Gamma, \Phi) = \int d(\lambda, \xi)\ |QCR\ U_\lambda(\Gamma, \Phi) X(\xi, \lambda)\|^2 \tag{46}$$

Augmenting with the "auxiliary field" gives

$$\tilde{\mathcal{O}}(\Gamma, \Phi, W) \quad = \quad \left(\|QCRW\|^2 + b\|W - U(\Gamma, \Phi)X(0)\|^2\right) \tag{47}$$

and we promote this objective to a parametric family of measures

$$-\log p_\Theta(W, \Gamma, \Phi) \quad \sim \quad \Theta\left(\|QCRW\|^2 + b\|W - U(\Gamma, \Phi)X(0)\|^2\right) + \log Z[\Theta, b] \tag{48}$$

Note - optimizing an objective is independent of an overall scalar (> 0, i.e. without sign change). "Marginalizing" over W is equivalent to evaluating at the optimal W (as a function of any DM setting)

$$\begin{aligned} \hat{W} &= (bI + M)^{-1} bUX(0) \\ &= \left[I - R^\dagger C^\dagger Q \left(bI + QCRR^\dagger CQ\right)^{-1} QCR\right] UX(0) \end{aligned} \tag{49}$$

(with $M = R^\dagger C^\dagger |Q|^2 CR$) giving

$$\begin{aligned} \tilde{\mathcal{O}} &= \|QCR\hat{W}\|^2 + b\|\hat{W} - U(\Gamma, \Phi)X(0)\|^2 \\ &= \hat{W}^\dagger (bI + M)\hat{W} - bX(0)U^\dagger \hat{W} - b\hat{W}^\dagger UX(0) + b|X(0)|^2 \\ &= b|X(0)|^2 - \hat{W}^\dagger (bI + M)\hat{W} \\ &= bX(0)U^\dagger \left[I - b(bI + R^\dagger C^\dagger |Q|^2 CR)^{-1}\right] UX(0) \\ &= bX(0)U^\dagger \left[I - \left(I - R^\dagger C^\dagger Q \left(bI + QCRR^\dagger C^\dagger Q\right)^{-1} QCR\right)\right] UX(0) \\ &= bX(0)U^\dagger \left[R^\dagger C^\dagger Q \left(bI + QCRR^\dagger C^\dagger Q\right)^{-1} QCR\right] UX(0) \end{aligned} \tag{50}$$

This gives the identity for our measures

$$\begin{aligned} -\log p_\Theta[\Gamma, \Phi] \quad &\sim \quad \Theta\ \mathcal{O}[\Gamma, \Phi, \hat{W}(\Gamma, \Phi)] + \log W[\Theta] - \frac{1}{2\Theta} \log\det\left|bI + R^\dagger C^\dagger |Q|^2 CR\right| \\ &\equiv \quad H(\Gamma, \Phi) + \text{state independent constants} \end{aligned} \tag{51}$$

APPENDIX D. CONVERGENCE TO LOCAL MINIMA

The auxiliary field optimization iteration is really a form of "expectation-maximization" As noted above, our on-axis dark hole energy objective function is "promoted to a probability on DM solutions along with auxiliary variables"

$$P[\Gamma, \Phi, W] \quad \propto \quad e^{-\beta \ \|QCW\|^2 - b\|W - U(\Gamma,\Phi)A\|^2} \tag{52}$$

and as noted this form is *designed* so that analytic integration over W leads to $-\log P \rightarrow_{b \gg 1} \beta \ \|QCU(\Gamma, \Phi)\|^2$. For any value of the regularization parameter 'b', the conditional $P[W|\Gamma, \Phi]$ is Gaussian with a "peak" at the field

$$\max_W \left(-\log P[W|\Gamma, \Phi]\right) \quad = \quad \left(bI + C^\dagger QC\right)^{-1} bU(\Gamma, \Phi)A \tag{53}$$

Jensen's inequality leads to the well known Expectation-Maximization iterative algorithm[6]

$$\begin{aligned} \log\left(\frac{P[\Gamma, \Phi]}{P[\Gamma_n, \Phi_n]}\right) \quad &\geq \quad \int dW \ P[W|\Gamma_n, \Phi_n] \ \log\left(\frac{P[\Gamma, \Phi|W]}{P[\Gamma_n, \Phi_n|W]}\right) \\ &= \quad -\int dW \ P[W|\Gamma_n, \Phi_n] \ \left(\|W - U(\Gamma, \Phi)A\|^2 - \|W - U(\Gamma_n, \Phi_n)A\|^2\right) \end{aligned}$$

The above shows that *maximizing the right-hand side never results in a worse objective (*$-\log P$. For the Gaussian (conditioned on (Γ_n, Φ_n)) maximizing the right-hand side equivalent to

$$\{\Gamma_{n+1}, \Phi_{n+1}\} \quad = \quad \min_{\Gamma, \Phi} \left(\left\|\hat{W}(\Gamma_n, \Phi_n) - \left(P_\lambda^\dagger e^{i(\lambda_0/\lambda)\Gamma} P_\lambda e^{i(\lambda_0/\lambda)\Phi}\right) A\right\|^2\right) \tag{54}$$

with $\hat{W}(\Gamma_n, \Phi_n)$ the mean field given the past DM solutions.

ACKNOWLEDGMENTS

We thank Matthew Bolcar (NASA Goddard Space Flight Center) for providing the aperture for the LUVOIR architecture 'A' design used in this paper. This work was partially performed at the Jet Propulsion Laboratory, California Institute of Technology , under contract with the National Aeronautics and Space Adminstration. Government sponsorship acknowledged. Copyright, 2017, all rights reserved.

REFERENCES

[1] Stark, C., Roberge, A., Mandell, A., and Robinson, T., "Maximizing the ExoEarth Candidate Yield From A Future Direct Imaging Mission," *Astrophys. J.* **795**, 122–141 (2014).

[2] Ruane, G., Jewell, J., Mawet, D., Pueyo, L., and Shaklan, S., "Apodized vortex coronagraph designs for segmented aperture telescopes," *Proc. SPIE* **9912**, 9912L (2016).

[3] Boyd, S. and Vandenberghe, L., [*Convex Optimization*], Cambridge University Press, Cambridge, U.K. (2009).

[4] Groff, T., Riggs, A. E., Kern, B., and Kasdin, N. J. ., "Methods and limitations of focal plane sensing, estimation, and control in high-contrast imaging," *J. Astron. Telesc. Instrum. Syst.* **2**(1), 011009 (2016).

[5] Mazoyer, J., Pueyo, L., N'Diaye, M., and et. al., "Correcting for the effects of pupil discontinuities with the ACAD method," *Proc. SPIE* **9904**, 9904T–1 (2016).

[6] Dempster, A., Laird, N. M., and Rubin, D., "Maximum Likelihood from Incomplete Data via the EM Algorithm," *J. R. Stat. Soc. B* **39**(1), 1–38 (1977).